ChemPlusChem

Research Article
doi.org/10.1002/cplu.202400510

Chemistry Europe
European Chemical Societies Publishing

www.chempluschem.org

Covalent Functionalisation of rGO and Nanodiamonds: Complementary Versatility and Applicability of Azomethine Ylide, Nitrile Oxide and Nitrone

Katia Martina,*[a] Silvia Tagliapietra,[a] Federica Calsolaro,[a] Andrei Paraschiv,[a] Mirko Sacco,[a] Federico Picollo,[b] Sofia Sturari,[b] Pietro Arpà,[b] Lorenzo Mino,[c] Alessandro Barge,[a] and Giancarlo Cravotto*[a]

The existing synthetic protocols for the direct functionalization of carbon-based nanomaterials often entail limitations due to their harsh reaction conditions, which require the use of high temperatures for extended periods. This study aims to overcome these limitations by developing mild and efficient synthetic protocols around 1,3-dipolar cycloaddition. Beginning with the well-established azomethine ylide derivatization, we progress to the utilization of nitrile oxide, and of nitrone derivatives for the functionalization of reduced graphene oxide (rGO) as well as of nanodiamonds (NDs). This comparative work employs both classical heating and microwave activation with the aim of reducing reaction times and enhancing efficacy. Results demonstrate that nitrone can react at 60 °C and that the reaction temperature may be decreased to 30 °C with nitrile oxide. Excellent progress was made in reducing the large excess of dipoles typically required for derivatization. Nitrile oxide was proved to be the most efficient in terms of derivatization degree, while nitrone was the most versatile reagent, facilitating the decoration of the carbon nanolayer with disubstituted dihydroisoxazole. To accurately assess the degree of functionalization, the reaction products underwent characterization using various spectroscopic and analytical techniques. Additionally, an indirect evaluation of the reaction outcome was conducted through Fmoc deprotection and quantification.

Introduction

Carbon-based nanomaterials have been intensively investigated over the past two decades, and their production is now highly dedicated to technological applications.[1] Biomedical applications, hydrogen storage, contaminant sequestration, electrocatalysis, fuel and solar cells, batteries, electromagnetic shields, conductive paints and reinforcement for polymers are just some of the wide range of studied applications.[2] Carbon nanomaterials are classified based on their allotropic structure and hybridization (sp^3, sp^2, sp), leading to diverse forms like diamond, graphite, and carbyne.[3]

Graphene offers distinct advantages, from an engineering standpoint, compared to CNT and fullerenes; its production yields a higher quality material with greater batch consistency, thus attracting stronger interest from industry. Great efforts have been made to improve the processability of graphene-based materials as low solubility, poor reactivity and limited accessibility have to be overcome before any chemical derivatization is possible.[4] Chemical exfoliation strategies, involving sequential oxidation and graphite reduction, yield a class of materials known as reduced graphene oxides (rGOs), which possess graphene-like characteristics.[5] rGO is a system characterized by graphene domains, defects and residual oxygen-containing groups on the surface of the sheets. It is dispersible in polar organic solvents, and thus potentially functionalized, thanks to enhanced reactivity stemming from the presence of defects associated with dangling bonds on the graphene lattice.[6]

NDs are composed of an sp^3 carbon structure surrounded by a shell consisting of functional groups. They exhibit a variety of sizes, shapes and surface chemistry that can be modulated by varying the synthetic approach.[7] ND-surface functional groups determine the chemical state of the carbon material, while their modification tunes both macroscopic and microscopic properties. Due to their non-toxic nature, these compounds have been extensively investigated for potential biomedical applications.[8]

Due to their high surface-to-volume ratio, the surface properties of NDs play an important role, and a range of different strategies have been pursued to grant the homogeneous and reactive distribution of surface species.[9]

[a] K. Martina, S. Tagliapietra, F. Calsolaro, A. Paraschiv, M. Sacco, A. Barge, G. Cravotto
Department of Drug Science and Technology, University of Turin, Via P. Giuria 9, 10125 Turin, Italy
E-mail: katia.martina@unito.it
giancarlo.cravotto@unito.it

[b] F. Picollo, S. Sturari, P. Arpà
Department of Physics and "NIS Inter-departmental Centre", National Institute of Nuclear Physics, University of Turin, 10125 Torino, Italy

[c] L. Mino
Department of Chemistry and NIS Interdepartmental Centre, University of Turin, Via Pietro Giuria 7, 10125 Turin, Italy

Supporting information for this article is available on the WWW under https://doi.org/10.1002/cplu.202400510

Chemical treatments can dramatically alter the properties of carbon-based nanomaterials by adding defects and impurities, by changing their structure and topology, and by affecting their mechanical properties, thermal conductivity and electrical conductivity.[10] Moreover, some imperfections may increase local reactivity and be exploited for certain applications to create defined properties and achieve new functionalities.[11] New studies have focused on functionalizing the carbonaceous network to modulate properties such as dispersibility in water and to enable new applications. Despite the high chemical inertness of the carbon-based nanomaterial, some notable examples of successful organic functionalization have been reported.[12] Direct covalent modification of the graphitic surface, without oxidation or any other pre-treatment, has attracted considerable interest, and these methods include 1,3-dipolar cycloadditions (1,3-DCA), which are a special class of organic reactions with demonstrated applicability in various experimental reports,[13] and several theoretical studies.[14] The design of nanomaterials with adaptability across a range of fields, including environmental, catalytic and biomedical applications, has historically presented a significant challenge. The introduction of covalent chemical modification by 1,3-DCA has the potential to address this challenge by introducing new chemical functionalities and enabling the direct grafting of desired molecular entities. As shown in Figure 1, 1,3-DCA alters the geometry and electronic structure of graphene by introducing localized sp^3 hybridization defects. Since the local bonding configuration significantly influences the physicochemical and structural properties of functionalized graphene, the 1,3-DCA strategy has been also demonstrated to enhance the solubility and processability of graphene.[15] Additionally, the dependence of the electronic properties on the degree of functionalization of graphene suggests its applicability for the production of new graphene-based nanoelectronic and nanophotonic devices.[15,16]

To date, the 1,3-DCA of azomethine ylides onto single-walled carbon nanotubes (SWCNTs), graphene, and nanodiamonds (NDs) has been extensively reported, leading to the production of functionalized and highly dispersed systems.[17] However, despite the potential of this field and the ongoing demand to introduce new functionalities into carbon-based networks, the exploration of other dipoles remains limited in the literature. There have been only several attempts to derivatize fullerene, graphene, SWCNTs and multi-walled (MW) CNT with nitrile oxide and pyrazolium ylides.[18] Additionally, there is very little literature on the use of nitrone for carbon-based nanomaterial derivatization for SWCNTs[19] and graphene quantum dots (GQDs).[20]

This study aims to develop and optimize mild, efficient synthetic protocols for 1,3-dipolar cycloadditions (1,3-DCA), starting with the well-known azomethine ylide derivatization and extending to nitrile oxide and nitrone derivatives. With the aim to further expand their potential applications, the focus is on adopting shared chemical pathways for the functionalization of reduced graphene oxide (rGO) and nanodiamonds (NDs), that integrate the carbon nanostructures into diverse microsystems.

The selection of nitrone and nitrile oxide as dipoles was strategically aligned with the goal of synthesizing dihydroisoxazole- and isoxazolidine-functionalized rGO and NDs.[21] This approach not only facilitates the introduction of diverse func-

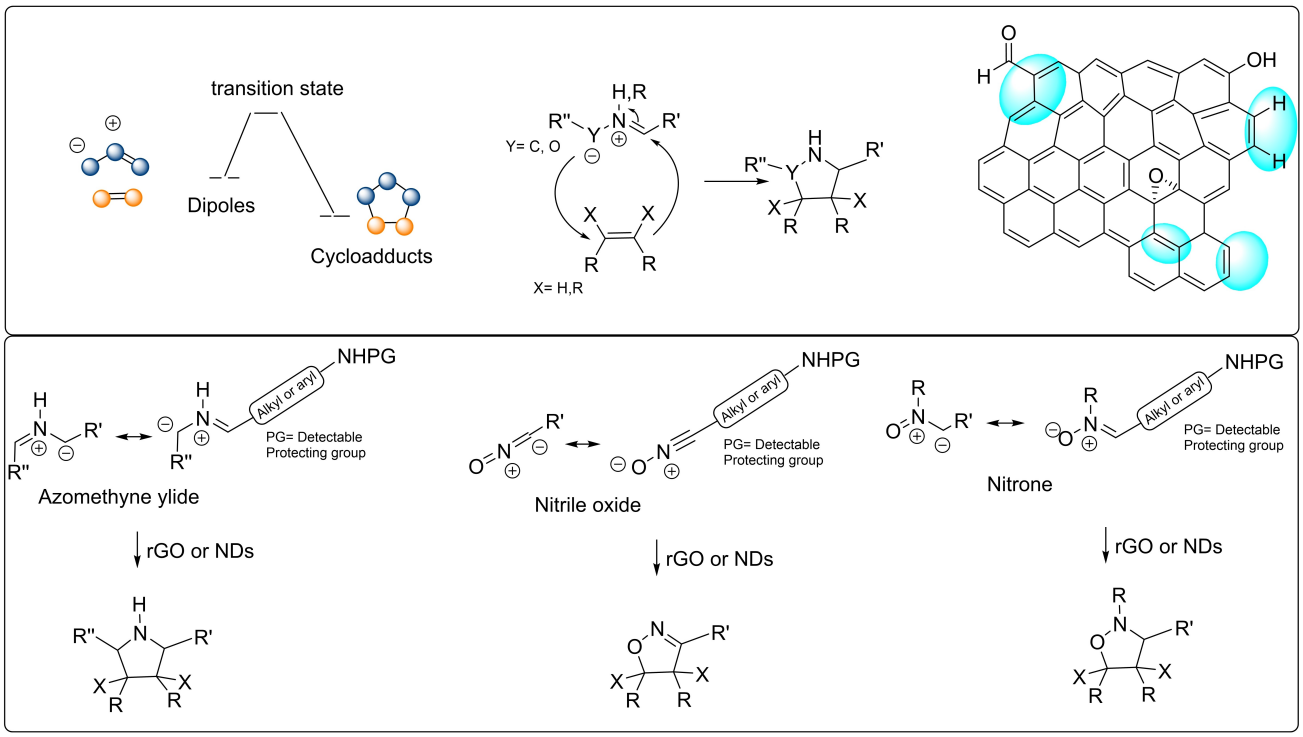

Figure 1. Graphical representation of 1,3 DCA: mechanism of reaction of 1,3-dipoles with C=C double bonds, representation of rGO and NDs surface reactivity and dipoles representation with reaction products.

tional groups through heteroatom doping on the carbon surface but also leverages the unique properties of isoxazolidine. Notably, isoxazolidine serves as a versatile masking agent for amino acids, amino alcohols, and β-diketones,[22] thereby enhancing the hydrophilicity of the carbon nanomaterial.

To achieve cost-effective derivatization of carbon nanomaterials, this study focuses on reducing reaction time and improving efficiency. Although 1,3-DCA is an effective approach, its application is often hindered by the necessity for elevated reaction temperatures and the use of large excesses of reagents, which significantly limit its practicality. In order to overcome these challenges, and drawing on previous studies of carbon-based nanomaterial functionalisation,[23] the use of microwave (MW) irradiation was investigated as a method to generate 1,3-dipoles in situ and to facilitate subsequent cycloadditions.[24]

In summary, this work presents a comparative study of three 1,3-dipolar cycloaddition (1,3-DCA) reactions, aiming to enhance their efficiency by minimizing reaction time, lowering reaction temperature, and reducing the excessive amounts of dipoles typically required. In order to carefully measure the functionalization degree, the reaction products were characterized using several spectroscopic and analytical techniques. An indirect evaluation of the reaction outcome was performed through Fmoc deprotection and quantification.

Results and Discussion

rGO offers a distinctive combination of properties in comparison to graphene and graphene oxide (GO), facilitating the modification process without compromising its electrical conductivity. In contrast to GO, rGO restores a significant proportion of its sp^2-hybridised carbon network, while simultaneously providing surface functional groups that enable its chemical reactivity and dispersion, a quality that is absent in pure graphene. NDs, on the other hand, are carbon-based materials with an sp^3-hybridized carbon structure, similar to bulk diamond. They have high surface areas, and through thermal annealing, non-diamond carbon (π-bonded carbon) can form around the diamond core. Despite their lower reactivity, functionalization techniques used for fullerenes and carbon nanotubes (CNTs) can also be applied to both rGO and NDs. The 1,3-DCA can be applied with the π-bonds of the sp^2 carbon atoms in the carbon lattice.[14c]

Since the surfaces of both rGO and NDs are not homogeneous, and graphene-like layers contain defects, introducing oxygen functional groups not only increases solubility but also adds functionalities that enhance the material's chemical reactivity.[25] Figure 1 illustrates the 1,3-DCA reaction pathways and highlights functional groups on rGO, alongside a selection of reactive structures on the annealed surface of NDs. The reaction of the 1,3-dipole and the dipolarophile results in the formation of a five-membered cycloadduct, accompanied by the loss of formal charges on the reactants.[26] This mechanism is based on a concerted cycloaddition reaction.[27] The analysis of binding energy demonstrated that the flat structure and perfect sp^2 hybridization of graphene render it less reactive than fullerenes and nanotubes. Nevertheless, the incorporation of Stone-Wales defects markedly augments its reactivity.[28] As reported, modifications on rGO are therefore expected to occur primarily at the edges and near the edges of the graphene structure,[14c,29] while the sp^2 shells of NDs react with dipoles. The reactivity of NDs is significantly influenced by the presence of other functional groups on their surface.[30]

The low reactivity of rGO and NDs makes measuring the degree of substitution a significant challenge in carbon-based nanomaterial chemistry. A literature survey has indicated that the operating procedures for carbon-based nanomaterial functionalization vary substantially from manuscript to manuscript. Although thermogravimetric analysis (TGA) is commonly used to measure the degree of substitution, its low selectivity has prompted chemists to perform a range of analyses, including also IR, TGA/MS, SEM, TEM, XPS etc. In order to selectively quantify the grafted derivative, we decided to apply the Fmoc methodology, which has been successfully demonstrated in solid-phase peptide synthesis, and compare it to TGA analysis.[31] As reported, the degree of functionalization can be measured indirectly by deprotecting a small amount of Fmoc-protected carbon-based nanomaterial derivatized with 20% (v/v) piperidine in DMF, which generates the dibenzofulvene–piperidine adduct.[32] This adduct can be quantified using UV-Vis spectroscopy (see Scheme 1). The spectrometric measurement is performed at 301.0 nm, which is the maximum absorption wavelength of the dibenzofulvene–piperidine adduct.

We preliminarily acquired rGO and NDs. rGO was produced in-house from naturally abundant graphite using a chemical oxidation method, followed by hydrazine reduction, based on a modified Hummers' method.[33] MW irradiation was employed to reduce the reaction time for the reduction step from 2 hours to 10 min (see SI and Figure S1). The rGO was characterized using FT-IR (Fourier Transform Infrared Spectroscopy), Raman spectroscopy and TGA, as described in Figure S2. On the other hand, the NDs consist of commercial synthetic ND (Adamas, NC, USA) produced via the detonation of carbon-based compounds. The diamond nanoparticles have a nominal primary particle size of 5 nm. This sample was annealed at a high temperature in an inert environment (2 h at 800 °C in N_2 flux) in order to reorganize the disordered sp^2/sp^3 phases,[34] and graphitize the amorphous carbon outer layers while preserving the diamond phase (see SI and Figure S3). Depending on the synthesis method, NDs can vary in size, and their surfaces typically contain oxygen functional groups, therefore the TEM analysis of the processed ND samples was also obtained to demonstrate their size distribution and morphology. As shown in Figure 2,

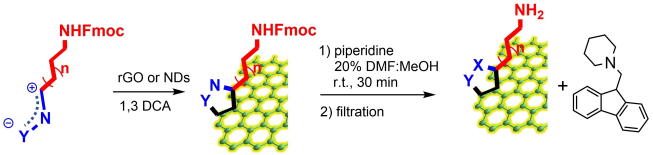

Scheme 1. Schematic representation of functionalization followed by Fmoc deprotection to obtain the fulvene – piperidine adduct in solution.

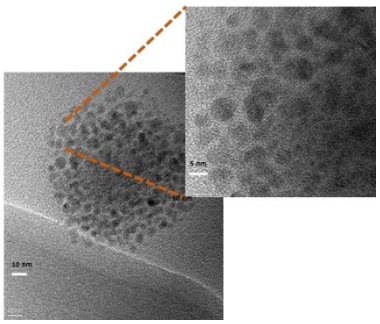

Figure 2. TEM of pristine nanodiamond.

the NDs exhibit a round shape with an average particle size of 5 nm, displaying high uniformity in both size and shape

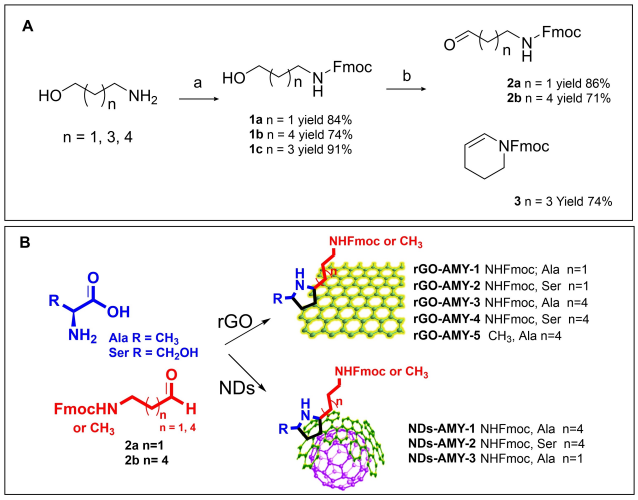

Scheme 2. A) Synthesis of Fmoc-aldehydes **2a**, **2b** and **3**. Reaction conditions a) Fmoc-OSu, DIPEA, DCM, r.t., 24 h; b) Dess-Martin periodinane, DCM, r.t., 90 min; B) Derivatization of rGO and NDs with azomethine ylides. Reaction conditions: aldehyde, amino acid, rGO or NDs, DMF, 2 h, 130 °C, MW.

The well-known functionalization method with azomethine ylides was tested under both conventional heating and MW irradiation, and the efficacy of the two heating methods in rGO and ND functionalization was compared. The use of MW, in fact, accelerates the preparation and derivatization of carbon-based materials due to the intense MW-material interactions.

Several Fmoc-protected alkyl aldehydes were synthesized, starting from their amino alcohol precursors (Scheme 2). Unfortunately, the main product yielded during the oxidation of 5-Fmoc-amino pentanol was the side product of the intramolecular cyclization of the aldehyde, resulting in cyclic enecarbamates **3** (Scheme 2A, see SI).[35]

rGO derivatization was performed, based on our experience with SWCNT, using Fmoc aldehydes **2a** and **2b**.[36] Dimethylformamide (DMF) was selected as the solvent of choice to minimize the interfacial tension between the solvent and graphene. Initial sonication was used to promote the exfoliation of the bulk material through acoustic cavitation. The reaction was carried out at 130 °C for 2 hours under MW irradiation (Scheme 2B).{Giofrè, 2020 #2} As described in Table 1, N-Fmoc amino propanal **2a** and N-Fmoc amino hexanal **2b** were reacted in the presence of alanine and serine. To prevent possible π-π interactions between the Fmoc portion and the rGO electronic cloud, the same reaction was performed using hexanal and alanine as azomethine ylide precursors (see Table 1). The efficiency of rGO functionalization was measured using TGA and, whenever possible, by UV measurement. Fmoc deprotection was performed using 3–5 mg of grafted rGO in a solution of piperidine (20% in DMA) and MeOH (1:1). After filtration, the resulting solution was analyzed by UV-vis spectroscopy at a wavelength of 301 nm (ε = 7800). The TGA analyses of pristine and grafted rGO were all normalized to 150 °C to circumvent any possible solvent influence on yield calculations. As described in Table 1, the results provided by TGA and UV measurements were in agreement, showing a range of 10–15% (w/w) functionalization when the reaction was performed in a MW oven. Lower derivatization was obtained when the reaction was heated in an oil bath, as confirmed by comparing the results with literature studies[23c]

Table 1. Functionalization degree of rGO and NDs via 1,3-DCA with azomethine ylides.

En.	Reaction conditions.	Sample	% UV % w/w (μmol/g)	% TGA % w/w (μmol/g)
1	Hexanal – Ala, oil bath	rGO-AMY-5[a]	n.d.	3.6 (476)
2	Hexanal – Ala; MW	rGO-AMY-5	n.d.	7.04 (580)
3	**2a** – Ala, MW	rGO-AMY-1	10.3 (329)	12.1 (387)
4	**2a** – Ser, MW	rGO- AMY-2	6.9 (180)	8.5 (221)
5	**2b** – Ala; MW	rGO-AMY-3	12.4 (340)	14.5 (397)
6	**2b** – Ser; MW	rGO-AMY4	10.1 (272)	11.8 (310)
7	**2b** – Ala; MW	NDs-AMY-1	3.5 (96)	3.8 (104)
8	**2b** – Ser; MW	NDs-AMY-2	4.2 (110)	4.7 (117)
9	**2a** – Ala; MW	NDs-AMY-3	2.3 (74)	2,5 (80)

Reaction conditions: 1.6 mmol aldehyde, 1.9 mmol amino acid, 50 mg rGO or NDs, DMF (13.3 mL), 2 h, 130 °C, MW; [a] conventional heating. n.d. means no detectable, due to the absence of Fmoc portion.

(see Table 1 entries 1 and 2, SI Figure S4A). When comparing the reactivities of compounds **2a** and **2b**, the latter exhibited a higher degree of functionalization, indicating that the longer chain enhanced the extent of functionalization. Given the significance of orbital overlap between the dipole and dipolarophile, we hypothesized that the azomethine ylide function's accessibility to the graphenic structure was improved with aldehyde **2b**. This enhancement may be attributed to the π-π interaction between the Fmoc group and graphene, which could reduce the availability of the dipole when the chain is shorter. Of the two amino acids tested, serine and alanine, Ala gave a higher degree of derivatization when rGO was reacted. The thermogram profiles are clearly comparable when shorter and longer chain N-Fmoc aldehydes are reacted with aa and rGO, with a higher degree of derivatization confirmed in the presence of derivative **2b** (see Table 1, entries 2–6). The TGA curves show that rGO exhibits constant weight loss under an inert atmosphere, whereas two degradation steps are observed when it is grafted; the first starts at 215 °C, while the second at 257 °C (see SI Figure S4B).

The excellent derivatization efficiency and quantification strategy led us to use the same methodology to study the feasibility of ND surface functionalization via 1,3-DCA (see Table 1 entries 7 and 8). The direct functionalization of NDs via 1,3-DCA was carried out using aldehydes **2a**, **2b**, and either alanine or serine, under microwave irradiation at 130 °C for 2 hours (Table 1, entries 7–9). As illustrated in the table, NDs demonstrated a comparatively diminished degree of functionalisation in comparison to rGO, which is likely attributable to the presence of disordered graphitic material exclusively on the ND surface. The efficiency of grafting is contingent upon the surface composition, with dipoles exhibiting reactivity towards C=C bonds and carbonyl groups.[37] While annealed NDs generally show higher functionalization, they still tend to have lower reactivity compared to rGO. Nonetheless, the degree of derivatization we observed was consistent and reproducible, aligning with previously reported 1,3-DCA functionalization of NDs.[38] This result can be attributed to the high quality of pristine NDs, which exhibited a large surface area and uniform size and shape, as illustrated in Figure 2.[38]

As shown in entries 7 and 9 of Table 1, a derivatization degree ranging from 2.3 % to 4.7 % (w/w), determined through TGA analysis, was achieved and confirmed by UV analysis, demonstrating the effectiveness of 1,3-DCA as a functionalization method (Table 1, entries 7 and 9; SI Figure S4C). It was observed that the Fmoc-protected aldehyde **2b** and serine resulted in a higher functionalisation degree, indicating that aldehyde **2a** was less efficient in derivatising NDs. This finding aligns with previous reports on the derivatisation of rGO (entry 9, Table 1). Furthermore, in contrast to rGO, the serine derivative was observed to exhibit a slightly higher efficiency in grafting the NDs surface than alanine, when entries 7 and 8 were compared. This behaviour may be correlated with the presence of oxygen-containing functional groups on the NDs surface, which allows the formation of hydrogen bonds with serine.[39] As also demonstrated by IR spectra of the starting carbon material (see SI Figure S2 and S3), the hydrophilicity of NDs is higher than that of rGO. This may prove the interesting variation of reactivity of rGO and NDs when hydrogen-donating functional groups are present on reagents.

The successful derivatization of azomethine ylides onto rGO and NDs surfaces was also confirmed by IR and DRIFT (Diffuse Reflectance Infrared Fourier Transform) spectroscopy. In the spectra of the pristine (see SI, Figure S3) and functionalized samples (see SI, Figure S5), we can readily recognize the vibrations of the pyrrolidine-derivatized carbon-based nanomaterial, in particular the ring-stretching modes in the 1500–1200 cm^{-1} spectral region, as reported in literature,[40] confirming the effectiveness of the functionalization procedure. Meanwhile, Raman spectroscopy confirms that sample processing barely perturbed the nanosystems, as demonstrated by the similarity between the spectra before and after surface modification. The only appreciable variation is the reduction in the intensity of the features at 1345–1580 cm^{-1} for the NDs (see SI Figure S5). A more detailed description of the main spectral features will be provided in the discussion of the FT-IR and Raman results of the nitrile oxide samples (vide infra).

Raman was also utilized to assess the efficacy of derivatization, as already reported in the literature.[41] Peak deconvolution was performed as exemplified in the Supporting Information (see Figure S6), and the full 1000–3500 cm^{-1} region of the spectrum was considered. Each peak was fitted using a multi-peak system based on relevant literature data, which evidenced the increase in satellite bands attributed to limit-sized sp^2 domains, proving covalent functionalization. The Raman degree of functionalization was measured, and an overestimated degree of functionalization was obtained compared to the TGA and UV measurements (see Table 3). As reported in Figure S6B, a G-band peak shift of functionalized rGO (**rGO-AMY-3**) was observed, compared to that of rGO, indicating the electronic effect of surface derivatization. We also recorded an increased band intensity I_D/I_G ratio (1.42 ± 0.04 versus 1.19 ± 0.05 for rGO) indicating increased defectiveness in the graphitic materials.

Despite the efficiency of azomethine ylide 1,3-DCA, this strategy has limitations; harsh reaction conditions and the limited availability of amino acid precursors. The studies reported in the literature on the derivatization of carbon-based nanomaterial include the use of nitrile oxide to derivatize fullerene, giving excellent results in short times under mild conditions by means of ultrasound irradiation or mechanochemical activation.[42] In order to investigate this process with rGO and NDs, the reaction was separately performed under MW activation and conventional heating at different reaction temperatures, with aromatic and aliphatic Fmoc-protected chloroximes being synthesized to provide the *in-situ* generation of nitrile oxides.

As reported in Scheme 3, alkyl Fmoc-amino protected chloroxime **5** was obtained from previously synthesized aldehyde **2b**. Since the 1,3-DCA reaction can follow either a concerted or stepwise mechanism, the interaction between the dipole and dipolarophile significantly influences the activation energy. As already reported in the literature, and described before we evidenced that the energy required to distort the 1,3-dipole and dipolarophile into the transition state geometry

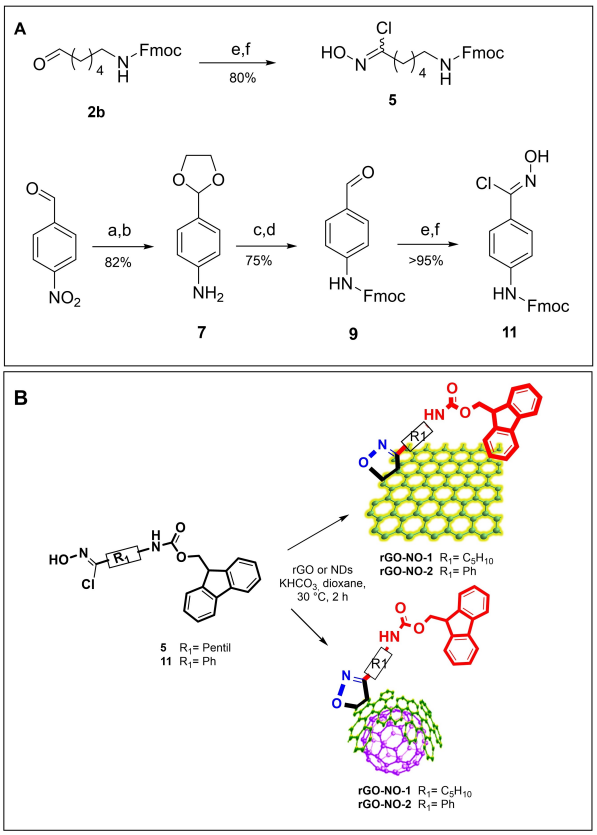

Scheme 3. A) Synthesis of Fmoc chloroximes **5** and **11** Reaction conditions: a) ethylene glycol, pTsOH, toluene reflux, 3 h; b) PtO_2, H_2, THF/EtOH, 20 °C, 1 h; c) Fmoc-Cl, pyridine, DCM, r.t., 3.5 h; d) *p*-TsOH, acetone/H_2O, r.t., 3 h; e) NH_2OH HCl, CH_3COONa, EtOH/THF, r.t., 3.5 h; f) NCS, DMF, r.t. 3 h. B) Derivatization of rGO and NDs with nitrile oxides generated *in situ* from chloroxime derivatives. Reaction conditions: chloroxime, rGO or NDs, $KHCO_3$, dioxane, 30 °C, 2 h

is a key factor in controlling the reactivity of 1,3-dipole cycloadditions with rGO and NDs.[14c] therefore the longer spacer between the aldehyde and Fmoc in derivative **2 b** was selected as a model. Also an aromatic chloroxime (**11**) was synthesized from the *p*-nitro benzaldehyde (see SI).

rGO functionalization was performed in dioxane with $KHCO_3$ and the reaction was repeated at different temperatures as described in Table 2. An excellent degree of functionalization was obtained in all reactions performed and, surprisingly, milder reaction conditions (30 °C, 2 h) gave rise to the best results, making these condition optimal. Interestingly, the amount of dipole could be reduced to one-fourth compared to the optimal protocol of azomethine ylide 1,3-DCA (see Table 2 entries 1, 4 and 5). Both aliphatic and aromatic chloroxime derivatives afforded the desired functionalization, and a slightly lower derivatization degree was measured for the aromatic analogue (17.8% versus 19.5%). Excellent results were obtained when NDs were subjected to derivatization via 1,3-DCA with nitrile oxide, with the degree of derivatization being almost three times higher than that achieved with azomethine ylide derivatization. The efficacy of this reaction demonstrated that not only could the reaction temperature be reduced, but also the reagent equivalents, compared to a recent example of nanotube derivatization with nitrile oxide 1,3 DCA function reported into the literature.[18e] The procedure proposed by Swager *et al.* in 2021 for the derivatization of more reactive SWCNTs employed a nine-fold reagent excess and a reaction temperature of 200 °C under MW irradiation.

TGA analyses of **rGO-NO-1** and **rGO-NO-2** consistently showed the presence of a single degradation step, starting at 183 °C for **rGO-NO-1** and at 149 °C for **rGO-NO-2** (Figure S7). A comparison of the pristine rGO FT-IR spectrum (Figure S2), which shows only minimal IR signals, with the spectra of the rGO-NO samples (Figure S8) confirms the success of the nitrile oxide functionalization. Specifically, we can identify the ν(N–H) and ν(C=O) vibrations of the carbamate group around 3400 and 1700 cm^{-1}, respectively.[43] Additionally, we note the presence of a band at about 1370 cm^{-1}, which has previously been attributed to N–O vibrations.[44] Similar spectroscopic features can also be recognized in derivatized ND samples. However, for these materials, the surface picture is more complex, as the spectra of pristine NDs show several IR signals, including bands attributed to ν(C–H), in the 3000–2800 cm^{-1} range, and to ν(C=O) at 1730 cm^{-1} (Figure S3 and S8), as previously discussed in detail in earlier studies.[39,45]

Table 2. Derivatization of rGO and NDs by 1,3-DCA with nitrile oxide.

En	Sample	Reaction Conditions	% UV % w/w (μmol/g)	% TGA % w/w (μmol/g)
1	rGO-NO-1	**5** (1,6 mmol), MW, 60 °C, 1 h	13.2 (285)	15.3 (453)
2	rGO-NO-1	**5** (0,8 mmol), MW, 60 °C, 1 h	14.6 (330)	16.3 (464)
3	rGO-NO-1	**5** (0,8 mmol), MW, 45 °C, 1 h	13.9 (342)	15.8 (450)
4	rGO-NO-1	**5** (0,8 mmol), o.b., 30 °C, 2 h	19.9 (484)	23.5 (649)
5	rGO-NO-1	**5** (0,42 mmol), o.b., 30 °C, 2 h	19.5 (482)	22.8 (649)
6	rGO-NO-2	**11** (0,42 mmol), o.b., 30 °C, 2 h	17.8(429	19.6 (546)
7	NDs-NO-1	**5** (0,42 mmol), o.b., 3 °C, 2 h	8.3 (204)	9.81 (376)
8	NDs-NO-2	**11** (0,42 mmol), o.b., 30 °C, 2 h	9.4 (247)	10.6 (294)

Reaction conditions: rGO or NDs (50 mg), chloroxime (mmols 1.6–0.42), $KHCO_3$ (0.417 mmol), dioxane (6.5 mL).

The Raman spectra of NDs are characterized by pronounced fluorescence, covering the investigated range and masking the presence of the D and G bands, located at 1345 cm^{-1} and 1580 cm^{-1}, respectively, which are still barely visible. The absence of the diamond-Raman peak is typical of diamond nanocrystals produced using the detonation technique, due both to the small dimensions of the diamond core and the presence of graphitic/amorphous superficial phases that reduce the intensity of the Raman signals.[39] In contrast, the spectra of the rGO samples present all the typical features of graphene-based materials; intense D and G bands, as well as 2D and 2 G (at 2700 cm^{-1} and 3180 cm^{-1}), which are ascribable to double resonance Dirac cone intravalley processes and the combination of these transitions (D + D″ at 2450 cm^{-1} and D + G at 2940 cm^{-1}). As is well known, several peaks (D, D′ at 1620 cm^{-1}, and D + D′ at 2800 cm^{-1}) are associated with the presence of structural defects in the rGO lattice, and are absent in a perfect graphene monolayer. These imperfections significantly affect the Raman response of the material, making an evaluation of the functionalization degree inaccurate when using the approach described by Rebelo *et al.* and Vecera *at al.*[41] This approach is based on the ratio between the integrated area of all the peaks previously described and the sum of the D and G areas (Chemical Functionalization Degree CFD). In fact, as already reported for the azomethyne ylide derivatization, the CFD measure by Raman is in disagreement with the TGA and UV absorption evaluations. When the derivatization was measured based on the I_D/I_G ratio, the covalent functionalization of rGO showed variable results; 1.34 ± 0.04 for **rGO-NO-1** and 1.20 ± 0.04 for **rGO-NO-2**. The significant difference between the derivatized rGO samples may be due to a combination of two factors; slightly lower derivatization of **rGO-NO-2**, as demonstrated by UV and TGA analyses, and the predominant aromatic substructure of nitrile oxide **11**.

The deep and extensive knowledge acquired on sp^2 graphitic surface functionalization via 1,3-DCA and the proven quantification method that uses Fmoc-amino protected derivatives as derivatizing agents were then utilized to directly functionalize rGO and NDs using another versatile cycloaddition reaction; the use of nitrones. This approach exploits eco-friendly and mild parameter conditions. Nitrones were chosen for their high reactivity towards dipolarophiles, while, compared to nitrile oxide, they allow two substituents to be substituted onto the oxazolidine ring, making this functionalization method suitable for the multifunctional derivatization of rGO and NDs.

The synthetic procedure for the synthesis of nitrones follows the reaction between hydroxylamines and aldehyde compounds. Aromatic hydroxylamine **13** (see Scheme 4) was prepared starting from its aldehyde precursor. It was then condensed with Fmoc-protected aldehydes **2 b** and **9** to obtain two nitrones with modulated alkyl and aryl substituents (**14** and **15**). Nitrones were synthesized in DCM in the presence of $MgSO_4$, as described in the literature.[46] The resulting dipoles were used in reactions without further purification. MS spectra were obtained to confirm the presence of the desired dipoles.

In order to assess the reactivity of these nitrones towards 1,3-DCA with rGO and NDs, the reaction was carried out in 1,4-dioxane, THF and toluene at different temperatures (see SI, Table S1). Unlike the procedure proposed in the literature with quantum dot graphene,[23d] we decided to reduce the amount of nitrone and maintained the same molar ratio (rGO or NDs/dipole) used for nitrile oxide 1,3-DCA. The derivatization degree was measured using indirect UV quantification after Fmoc deprotection and TGA. Gratifyingly, both rGO and ND functionalization were successful in toluene at 90 °C for 16 h. Under MW irradiation, a satisfactory derivatization degree was obtained in dioxane at 60 °C after 1 h (see Table S1, entries 1–5 for reaction optimization). Since toluene is a low microwave-adsorbing solvent, it was replaced with 1,4 dioxane to achieve comparable results. In dioxane, after 1 h of irradiation at 60 °C, the derivatization degree (w/w%) was slightly higher than that of conventional heating in toluene o.n. for rGO derivatization. In contrast, comparable and slightly lower derivatization degrees were obtained for MW-heated NDs (see Figure 1). When the reaction time was increased to 2 h, we did not observe an increased functionalization percentage. Interestingly, when the reaction was repeated in the presence of nitrones **14** and **15**, an interesting derivatization trend was obtained (see Scheme 4 and Figure 3). The nitrone obtained from aromatic aldehydes **15** (**rGO-Ntr-2**) showed lower reactivity than that obtained from derivative **14** (**rGO-Ntr-1**). Despite the variable degree of functionalization, the overall efficacy of the methodology was demonstrated, with a w/w % of functionalization on rGO ranging from 4–12 %. These results are not only comparable to, or higher than, those in previous studies, but they also allow access to derivatized rGO under milder conditions. When the reaction was repeated with NDs, a satisfactory derivatization degree was measured, confirming the same trend. Nitrone **15** had a lesser effect on the degree of functionalization (ND derivatization range from 3.7–5.2 % w/w, see Table S1).

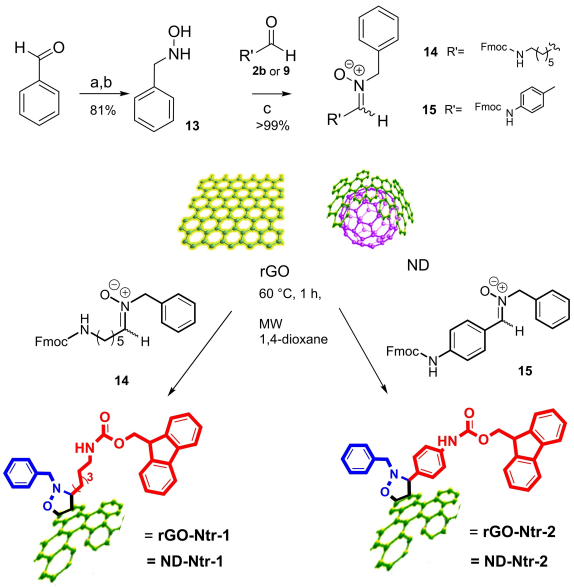

Scheme 4. Synthesis of nitrones **14–15** Reaction conditions: a) $NH_2OH{\cdot}HCl$, base, EtOH, b) $NaBH_3CN$, MeOH, r.t., c) $NaHCO_3$, Na_2SO_4, DCM. Derivatization of rGO and NDs with nitrones.

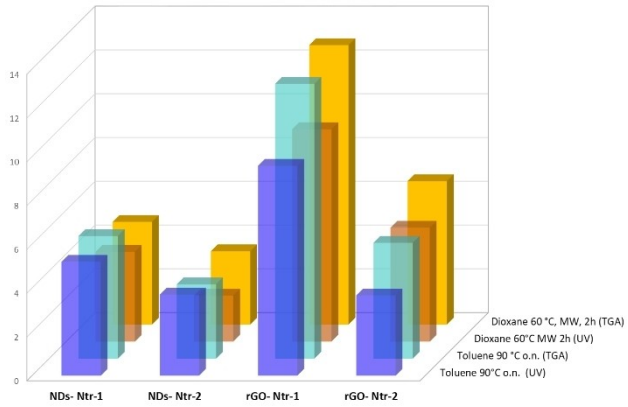

Figure 3. Degree of derivatization of rGO and NDs-Nitr-1 and 2 under oil bath or MW heating.

The effectiveness of the derivatization reactions was proven using TGA, FT-IR and DRIFT, and Raman spectroscopy.

The TGA curves of the cycloadducts showed a degradation step that started approximately at 216 °C for rGO derivatives, while the TGA of NDs indicated increased thermal stability with the degradation step starting at 284 °C (Figure S10). As with the nitrile oxide, IR spectroscopy (Figure S11) confirms the successful derivatization of the samples, which is demonstrated by the presence of the carbonyl-group stretching vibration around 1700 cm^{-1} and carbon–carbon bonds in the aromatic rings in the 1600–1400 cm^{-1} spectral region.[47] Analogously to nitrile oxide functionalization, derivatization with nitrone has a low impact on Raman spectra for both NDs and rGO. This confirms that the developed chemistry route does not modify the structure of the carbon-based nanomaterial while allowing the desired surface modification to proceed.

A comprehensive view of the rGO-derivatization degree when reactions were performed using 1,3-DCA is described in Table 3. As can be observed, the Raman degree of derivatization for rGO ranged between 22 and 21%, indicating successful derivatization. However based on Raman data, the CFD is overestimated, and we could not observe the variable degree of surface modification that was measured by UV and TGA. The reason for this trend may be the presence of defects on the surface of pristine rGO. By measuring the ratio of Raman I_D/I_G bands, we were able to observe the trend of chemical derivatization; both **rGO-NO-1** and **rGO-Ntr-1** are higher in degree than **rGO-NO-2** and **rGO-Ntr-2**. We must also underline the fact that starting dipoles **11** and **15**, employed to obtain derivatives **rGO-NO-2** and **rGO-Ntr-2**, already displayed an aromatic structure.

Table 3. Chemical functionalization degree of 1,3 DCA on rGO obtained by Raman, TGA and UV. a) Chemical functionalization degree (CFD) calculated on the basis of Raman deconvolution.

Sample	% TGA	% UV	% CFD[a]	I_d/I_g
rGO-AMY-3	14,5	12,4	22,3	1.40
rGO-NO-1	22,8	19,5	29	1.34
rGO-NO-2	19,6	17,8	25,5	1.20
rGO-Ntr-1	12,76	9,7	21,9	1.52
rGO-Ntr-2	6,55	5,2	22,2	1.21

Conclusions

In conclusion, this study describes efficient procedures for the 1,3-DCA derivatization of rGO and NDs. To accurately assess the degree of functionalization, the reaction products underwent characterization using various spectroscopic and analytical techniques. Additionally, an indirect evaluation of the reaction outcome was conducted using Fmoc deprotection and quantification. Comparing the AMY, Ntr, and NO dipoles reveals differences in reaction conditions and the extent of derivatization. All approaches effectively modified the surface of carbon-based nanomaterials, with reaction temperatures ranging from 130 °C for AMY to 30 °C for NO. Of these, NO proved to be the most efficient in terms of derivatization degree, while Ntr was the most versatile reagent, facilitating the decoration of the carbon nanolayer with disubstituted dihydroisoxazole. Microwave irradiation accelerated reaction rates during the reactions involving AMY and Ntr. In summary, reaction time, temperature, and reagent amounts were carefully optimized to achieve excellent results under mild and efficient conditions. The versatility of this approach and its capacity to produce highly functionalised carbon materials, ranging from rGO to NDs, through a single-step protocol, are well established. In this study, we demonstrate that derivatisation using nitrone and nitrile oxide provides an economical, rapid, and efficient route to obtaining pure hydrophilic carbon nanomaterials, which can be exploited for a variety of applications. Moreover, the fact that this method can be carried out in the presence of thermolabile biomolecules makes it a promising candidate for biomedical applications, and it is therefore worthy of further investigation in this field.

Acknowledgements

The University of Turin is warmly acknowledged for its financial support (Rilo 2022). Open Access publishing facilitated by Università degli Studi di Torino, as part of the Wiley - CRUI-CARE agreement.

Conflict of Interests

The authors declare no conflict of interest.

Data Availability Statement

The data that support the findings of this study are available in the supplementary material of this article.

Keywords: Reduced graphene oxide · Nanodiamonds · Microwave · FMoc quantification · Dipole

[1] a) N. Rao, R. Singh, L. Bashambu, *Mater. Today Proc.* **2021**, *44*, 608–614; b) R. Manikandan, T. Rajarathinam, S. Jayaraman, H.-G. Jang, J.-H. Yoon, J. Lee, H.-j. Paik, S.-C. Chang, *Coord. Chem. Rev.* **2024**, *499*, 215487; c) B. Wang, P. Huang, B. Li, Z. Wu, Y. Xing, J. Zhu, L. Liu, *Small* **2023**, *19*, 2304246.

[2] a) A. Thakur, A. Kumar, A. Singh, *Carbon* **2024**, *217*, 118621; b) B. Li, X. Xie, T. Meng, X. Guo, Q. Li, Y. Yang, H. Jin, C. Jin, X. Meng, H. Pang, *Food Chem.* **2024**, *440*, 138213; c) J. Wang, Y. Fu, Z. Gu, H. Pan, P. Zhou, Q. Gan, Y. Yuan, C. Liu, *Small* **2024**, *20*, 2303773; d) D. Kumar, J. E. Abraham, M. Varghese, J. George, M. Balachandran, J. Cherusseri, *Int. J. Hydrogen Energy* **2024**, *50*, 118–141; e) X. Shi, S. Chen, *ChemPlusChem* **2023**, *88*, e202300008.

[3] R. B. Heimann, S. E. Evsvukov, Y. Koga, *Carbon* **1997**, *35*, 1654–1658.

[4] a) R. S. Sundaram, in *Graphene* (Eds.: V. Skákalová, A. B. Kaiser), Woodhead Publishing, Cambridge, **2014**, pp. 50–80; b) T. Gatti, N. Vicentini, M. Mba, E. Menna, *Eur. J. Org. Chem.* **2016**, *2016*, 1071–1090.

[5] O. C. Compton, S. T. Nguyen, *Small* **2010**, *6*, 711–723.

[6] a) F. Banhart, J. Kotakoski, A. V. Krasheninnikov, *ACS Nano* **2011**, *5*, 26–41; b) P. T. Araujo, M. Terrones, M. S. Dresselhaus, *Mater. Today* **2012**, *15*, 98–109; c) D. Boukhvalov, M. Katsnelson, *Nano Lett.* **2008**, *8,* 4373-4379; d) S. Mantovani, A. Pintus, A. Kovtun, G. Bertuzzi, M. Melucci, M. Bandini, *Eur. J. Org. Chem.* **2023**, *26*, e202300641.

[7] a) S. Stehlik, T. Glatzel, V. Pichot, R. Pawlak, E. Meyer, D. Spitzer, B. Rezek, *Diamond Relat. Mater.* **2016**, *63*, 97–102; b) E. Mayerhoefer, A. Krueger, *Acc. Chem. Res.* **2022**, *55*, 3594–3604; c) I. I. Kulakova, *Phys. Solid State* **2004**, *46*, 636–643.

[8] a) G. Reina, L. Zhao, A. Bianco, N. Komatsu, *Angew. Chem. Int. Ed.* **2019**, *58*, 17918–17929; b) F. Pan, M. Khan, A. H. Ragab, E. Javed, H. A. Alsalmah, I. Khan, T. Lei, A. Hussain, A. Mohamed, A. Zada, M. Z. Ansari, *Mater. Des.* **2023**, *233*, 112179; c) Z. Yang, T. Xu, H. Li, M. She, J. Chen, Z. Wang, S. Zhang, J. Li, *Chem. Rev.* **2023**, *123*, 11047–11136; d) Y.-L. Chen, G.-Y. Lee, M.-Y. Sung, J.-H. Huang, E.-C. Cho, K.-C. Lee, *ACS Appl. Mater. Interfaces* **2021**, *13*, 39088–39099; e) N. D. Yates, M. R. Dowsett, P. Bentley, J. A. Dickenson-Fogg, A. Pratt, C. F. Blanford, M. A. Fascione, A. Parkin, *Langmuir* **2020**, *36*, 5654–5664.

[9] a) C. Guo, J. Zheng, H. Deng, P. Shi, G. Zhao, *Carbon* **2021**, *175*, 454–466; b) M. Nishikawa, M. Liu, T. Yoshikawa, H. Takeuchi, N. Matsuno, N. Komatsu, *Carbon* **2023**, *205*, 463–474; c) C. Fessele, S. Wachtler, V. Chandrasekaran, C. Stiller, T. K. Lindhorst, A. Krueger, *Eur. J. Org. Chem.* **2015**, *2015*, 5519–5525.

[10] a) S. Kang, S. Ha, K. Kim, Y. Lee, Y.-J. Jang, J. Kim, K. Lee, H. J. Kim, *J. Mater. Res. Techn.* **2023**, *26*, 6027–6040; b) T. Tegafaw, S. Liu, M. Y. Ahmad, A. K. Ali Al Saidi, D. Zhao, Y. Liu, H. Yue, S.-W. Nam, Y. Chang, G. H. Lee, *RSC Adv.* **2023**, *13*, 32381–32397.

[11] a) L. Liu, M. Qing, Y. Wang, S. Chen, *J. Mater. Sci. Technol.* **2015**, *31*, 599–606; b) K. Guo, N. Li, L. Bao, P. Zhang, X. Lu, *Chem. Eng. J.* **2023**, *466*, 143060; c) S. Settele, F. J. Berger, S. Lindenthal, S. Zhao, A. A. El Yumin, N. F. Zorn, A. Asyuda, M. Zharnikov, A. Högele, J. Zaumseil, *Nat. Commun.* **2021**, *12*, 2119.

[12] a) M. Quintana, E. Vazquez, M. Prato, *Acc. Chem. Res.* **2013**, *46*, 138–148; b) D. Mosconi, M. Blanco, T. Gatti, L. Calvillo, M. Otyepka, A. Bakandritsos, E. Menna, S. Agnoli, G. Granozzi, *Carbon* **2019**, *143*, 318–328.

[13] a) E. Cunha, H. Ren, F. Lin, I. A. Kinloch, Q. Sun, Z. Fan, R. J. Young, *RSC Adv.* **2018**, *8*, 33564–33573; b) V. Georgakilas, A. B. Bourlinos, E. Ntararas, A. Ibraliu, D. Gournis, K. Dimos, A. Kouloumpis, R. Zboril, *Carbon* **2016**, *110*, 51–55; c) G. Neri, A. Scala, E. Fazio, P. G. Mineo, A. Rescifina, A. Piperno, G. Grassi, *Chem. Sci.* **2015**, *6*, 6961–6970.

[14] a) T. Yang, X. Zhao, S. Nagase, *J. Comput. Chem.* **2013**, *34*, 2223–2232; b) X. Lu, F. Tian, X. Xu, N. Wang, Q. Zhang, *J. Am. Chem. Soc.* **2003**, *125*, 10459–10464; c) Y. Cao, K. N. Houk, *J. Mater. Chem.* **2011**, *21*, 1503–1508.

[15] Q. Tang, Z. Zhou, Z. Chen, *Nanoscale* **2013**, *5*, 4541–4583.

[16] a) K. Suggs, D. Reuven, X.-Q. Wang, *J. Phys. Chem. C* **2011**, *115*, 3313–3317; b) B. Ou, R. Huang, W. Wang, H. Zhou, C. He, *RSC Adv.* **2014**, *4*, 43212–43219; c) T. Giousis, P. Zygouri, N. Karouta, K. Spyrou, M. Subrati, D. Moschovas, M. C. A. Stuart, H. Hemmatpour, D. P. Gournis, P. Rudolf, *Small* **2024**, *20*, 2403277.

[17] a) L. Basta, A. Moscardini, F. Fabbri, L. Bellucci, V. Tozzini, S. Rubini, A. Griesi, M. Gemmi, S. Heun, S. Veronesi, *Nanoscale Adv.* **2021**, *3*, 5841–5852; b) M. Garrido, L. Gualandi, S. Di Noja, G. Filippini, S. Bosi, M. Prato, *Chem. Commun.* **2020**, *56*, 12698–12716; c) P. Mehra, A. Paul, *J. Phys. Chem. C* **2022**, *126*, 6135–6146.

[18] a) M. Popławska, G. Z. Żukowska, S. Cudziło, M. Bystrzejewski, *Carbon* **2010**, *48*, 1318–1320; b) M. S. Meier, M. Poplawska, *Tetrahedron* **1996**, *52*, 5043–5052; c) A. P. Herman, S. Boncel, *RSC Adv.* **2016**, *6*, 64129–64132; d) M. Alvaro, P. Atienzar, P. de la Cruz, J. L. Delgado, V. Troiani, H. Garcia, F. Langa, A. Palkar, L. Echegoyen, *J. Am. Chem. Soc.* **2006**, *128*, 6626–6635; e) S.-X. L. Luo, R. Y. Liu, S. Lee, T. M. Swager, *J. Am. Chem. Soc.* **2021**, *143*, 10441–10453; f) H. Uceta, M. Vizuete, J. R. Carrillo, M. Barrejón, J. L. G. Fierro, M. P. Prieto, F. Langa, *Chem. Eur. J.* **2019**, *25*, 14644–14650.

[19] a) G. Ghini, L. Luconi, A. Rossin, C. Bianchini, G. Giambastiani, S. Cicchi, L. Lascialfari, A. Brandi, A. Giannasi, *Chem. Commun.* **2010**, *46*, 252–254; b) G. Giambastiani, S. Cicchi, A. Giannasi, L. Luconi, A. Rossin, F. Mercuri, C. Bianchini, A. Brandi, M. Melucci, G. Ghini, P. Stagnaro, L. Conzatti, E. Passaglia, M. Zoppi, T. Montini, P. Fornasiero, *Chem. Mater.* **2011**, *23*, 1923–1938.

[20] S. V. Giofrè, M. Tiecco, C. Celesti, S. Patanè, C. Triolo, A. Gulino, L. Spitaleri, S. Scalese, M. Scuderi, D. Iannazzo, *Nanomaterials (Basel)* **2020**, *10*, 2549.

[21] G. Speranza, *Nanomaterials* **2021**, *11*, 967-1066.

[22] a) C. Kashima, Y. Yamamoto, Y. Tsuda, *J. Org. Chem.* **1975**, *40*, 526–527; b) D. P. Curran, *J. Am. Chem. Soc.* **1983**, *105*, 5826–5833.

[23] a) Y. Wang, Z. Iqbal, S. Mitra, *Carbon* **2005**, *43*, 1015–1020; b) S. Tagliapietra, G. Cravotto, E. C. Gaudino, S. Visentin, V. Mussi, *Synlett* **2012**, *23*, 1459–1462; c) F. G. Brunetti, M. A. Herrero, J. d. M. Muñoz, S. Giordani, A. Díaz-Ortiz, S. Filippone, G. Ruaro, M. Meneghetti, M. Prato, E. Vázquez, *J. Am. Chem. Soc.* **2007**, *129*, 14580–14581; d) S. V. Giofrè, M. Tiecco, C. Celesti, S. Patanè, C. Triolo, A. Gulino, L. Spitaleri, S. Scalese, M. Scuderi, D. Iannazzo, *Nanomaterials* **2020**, *10*, 2549.

[24] a) K. Martina, S. Tagliapietra, V. V. Veselov, G. Cravotto, *Front. Chem.* **2019**, *7*, 95; b) J. Plumet, *ChemPlusChem* **2020**, *85*, 2252–2271.

[25] a) A. Z. Jovanović, A. S. Dobrota, N. V. Skorodumova, I. A. Pašti, *FlatChem* **2023**, *42*, 100573; b) M. B. Singh, P. Jain, F. Mohammad, P. Singh, I. Bahadur, O. P. Abedigamba, *ACS Omega* **2024**, *9*, 16458–16468.

[26] S. E. Beutick, P. Vermeeren, T. A. Hamlin, *Chem. – An Asian J.* **2022**, *17*, e202200553.

[27] a) K. V. Gothelf, K. A. Jørgensen, *Chem. Rev.* **1998**, *98*, 863–910; b) K. N. Houk, J. Sims, R. E. Duke, R. W. Strozier, J. K. George, *J. Am. Chem. Soc.* **1973**, *95*, 7287–7301.

[28] P. A. Denis, F. Iribarne, *Int. J. Quantum Chem.* **2010**, *110*, 1764–1771.

[29] a) I. K. Petrushenko, *Monatshefte für Chem. – Chem. Monthly* **2014**, *145*, 891–896; b) V. Shukla, *Nano. Adv.* **2020**, *2*, 962–990.

[30] F. Ducrozet, H. A. Girard, J. Leroy, E. Larquet, I. Florea, E. Brun, C. Sicard-Roselli, J.-C. Arnault, *Nanomaterials* **2021**, *11*, 2671–2687.

[31] a) S. Eissler, M. Kley, D. Bächle, G. Loidl, T. Meier, D. Samson, *J. Pept. Sci.* **2017**, *23*, 757–762; b) J. Li, M. J. Vergne, E. D. Mowles, W.-H. Zhong, D. M. Hercules, C. M. Lukehart, *Carbon* **2005**, *43*, 2883–2893.

[32] J. E. Sheppeck, H. Kar, H. Hong, *Tetrahedron Lett.* **2000**, *41*, 5329–5333.

[33] M. Monajati, S. Borandeh, A. Hesami, D. Mansouri, A. M. Tamaddon, *Chem. Eng. J.* **2018**, *354*, 1153–1163.

[34] S. Osswald, G. Yushin, V. Mochalin, S. O. Kucheyev, Y. Gogotsi, *J. Am. Chem. Soc.* **2006**, *128*, 11635–11642.

[35] C. Yu, L. Hu, *Tetrahedron Lett.* **2001**, *42*, 5167–5170.

[36] E. Calcio Gaudino, S. Tagliapietra, K. Martina, A. Barge, M. Lolli, E. Terreno, D. Lembo, G. Cravotto, *Org. Biomol. Chem.* **2014**, *12*, 4708–4715.

[37] A. Krueger, *J. Mater. Chem.* **2008**, *18*, 1485–1492.

[38] D. Lang, A. Krueger, *Diamond Relat. Mater.* **2017**, *79*, 102–107.

[39] P. Aprà, L. Mino, A. Battiato, P. Olivero, S. Sturari, M. C. Valsania, V. Varzi, F. Picollo, *Nanomaterials* **2021**, *11*, 2740.

[40] d. N. D. Marcia Cordes, J. L. Walter, *Spectrochim. Acta, Part A* **1968**, *24*, 237–252.

[41] a) S. L. H. Rebelo, A. Guedes, M. E. Szefczyk, A. M. Pereira, J. P. Araújo, C. Freire, *Phys. Chem. Chem. Phys.* **2016**, *18*, 12784–12796; b) P. Vecera, J. C. Chacón-Torres, T. Pichler, S. Reich, H. R. Soni, A. Görling, K. Edelthalhammer, H. Peterlik, F. Hauke, A. Hirsch, *Nat. Commun.* **2017**, *8*, 15192.

[42] J. Safaei-Ghomi, R. Masoomi, *Ultrason. Sonochem.* **2015**, *23*, 212–218.

[43] N. B. Colthup, L. H. Daly, S. E. Wiberley, in *Introduction to Infrared and Raman Spectroscopy* (Third Edition) (Eds.: N. B. Colthup, L. H. Daly, S. E. Wiberley), Academic Press, San Diego **1990**, pp. 339–354.

[44] R. H. Wiley, B. J. Wakefield, *J. Org. Chem.* **1960**, *25*, 546–551.

[45] F. Picollo, L. Mino, A. Battiato, S. Ditalia Tchernij, J. Forneris, K. Martina, M. Sacco, S. Tagliapietra, E. Vittone, P. Olivero, A. Barge, *Diamond Relat. Mater.* **2019**, *91*, 22–28.

[46] P. Aschwanden, D. E. Frantz, E. M. Carreira, *Org. Lett.* **2000**, *2*, 2331–2333.
[47] N. B. Colthup, L. H. Daly, S. E. Wiberley, in *Introduction to Infrared and Raman Spectroscopy* (Third Edition) (Eds.: N. B. Colthup, L. H. Daly, S. E. Wiberley), Academic Press, San Diego **1990**, pp. 261–288.
[48] a) A. Boudhar, W. Ng Xiao, Y. Loh Chiew, N. Chia Wan, M. Tan Zhi, F. Nosten, W. Dymock Brian, S. W. Tan Kevin, *Antimicrob. Agents Chemother.* **2016**, *60*, 3076–3089; b) J. Nakamura, H. Yamashiro, S. Hayashi, M. Yamamoto, K. Miura, S. Xu, T. Doi, H. Maki, O. Yoshida, H. Arimoto, *Chem. Eur. J.* **2012**, *18*, 12681–12689; c) H. Park, Y. Kwon, J. E. Shin, W.-J. Kim, S. Hwang, S. Lee, S. Kim, *Synthesis* **2017**, *49*, 2761–2767; d) J. D. More, N. S. Finney, *Org. Lett.* **2002**, *4*, 3001–3003; e) P. Fischer, M. Morris, H. Müller-Bunz, P. Evans, *Eur. J. Org. Chem.* **2020**, *2020*, 1165–1176; f) R. Walton, P. M. Lahti, *Synth. Commun.* **1998**, *28*, 1087–1092; g) T. Okita, K. K. Asahara, K. Muto, J. Yamaguchi, *Org. Lett.* **2020**, *22*, 3205–3208; h) R. M. Pérez-García, G. Grønnevik, P. J. Riss, *Org. Lett.* **2021**, *23*, 1011–1015; i) S. Park, J. An, J. R. Potts, A. Velamakanni, S. Murali, R. S. Ruoff, *Carbon* **2011**, *49*, 3019–3023.

Manuscript received: August 26, 2024
Revised manuscript received: December 10, 2024
Accepted manuscript online: December 12, 2024
Version of record online: ■■, ■■

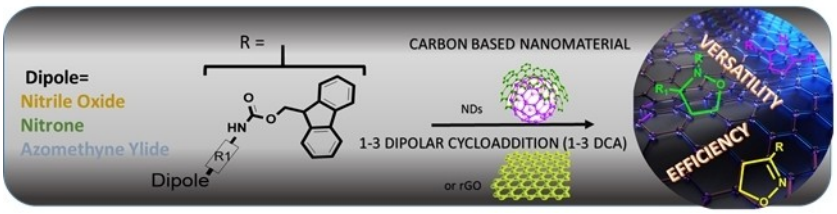

K. Martina, S. Tagliapietra, F. Calsolaro, A. Paraschiv, M. Sacco, F. Picollo, S. Sturari, P. Arpà, L. Mino, A. Barge, G. Cravotto**

1 – 11

Covalent Functionalisation of rGO and Nanodiamonds: Complementary Versatility and Applicability of Azomethine Ylide, Nitrile Oxide and Nitrone

1,3-DCA of nitrone and nitrile oxide to carbon based nanomaterial has been adapted from rGO to yield more stable, unique and biocompatible NDs. This strategy provides an economical, rapid, and efficient method for the production of pure, hydrophilic carbon nanomaterials, which are suitable for a wide range of applications.